POLITECNICO
MILANO 1863

SCUOLA DI INGEGNERIA INDUSTRIALE
E DELL'INFORMAZIONE

Executive Summary of the Thesis

Design, Fabrication and Mechanical Characterization of Fused Silica Microstructures by Two-Photon Polymerization

Laurea Magistrale in Materials and Nanotechnology Engineering

Author: Eugenio Spagnolo

Advisor: Prof. Laura Maria Vergani

Co-advisor: Eng. Federica Buccino, Eng. Christian Minnert, Dr. Prof. Jakob Schwiedrzik

Academic year: 2024-2025

1. Introduction

Fused silica is a widely used model amorphous ceramic for mechanical studies because its chemistry and structure are highly uniform, providing a reproducible baseline where strength variations mainly reflect flaws, surface condition, and size effects. It also combines excellent thermal, chemical, and optical stability with an intrinsically brittle mechanical response. [1]
At the macroscopic scale, measured strength is rarely an intrinsic material constant because it is controlled by the statistical distribution of surface and bulk flaws. When the characteristic dimensions shrink to the micrometer range, the stressed volume decreases and the probability of sampling a critical defect is reduced, so the apparent strength can increase toward near-intrinsic limits. This widely observed trend is often summarized by the heuristic "smaller is stronger", which motivates microscale testing and benchmarking. It can be rationalized in probabilistic terms through Weibull-type failure statistics:

$$P_f = 1 - \exp\left[-\left(\frac{\sigma}{\sigma_0}\right)^m\right], \qquad (1)$$

where σ_0 and m are material-dependent parameters and P_f increases with the applied stress σ for a given flaw population. [2, 3]
In parallel, additive manufacturing at the micro- and nanoscale enables the fabrication of microarchitected solids and test structures with high geometric freedom. Among available techniques, Two-Photon Polymerization (2PP) is particularly attractive because it combines submicrometric resolution with true 3D patterning. In 2PP, a tightly focused femtosecond near-infrared laser is scanned within a photosensitive resin; polymerization is triggered only where two-photon absorption occurs, i.e., in the high-intensity focal volume. This nonlinear absorption confines curing to a sub-micrometric *voxel*, enabling true volumetric writing and allowing feature size and bonding quality to be tuned through the delivered dose and the voxel overlap between adjacent scan lines and layers. [4]
A schematic of voxel formation and the resulting confinement principle is shown in Figure 1.
When coupled with silica-loaded photoresists such as GP-Silica, 2PP can produce polymer-derived glass microstructures after thermal conversion (debinding and sintering). However, a key bottleneck still limits quantitative mi-

croscale mechanics on 2PP-derived fused silica: achieving reproducible geometries and defect populations across printing sessions, environmental conditions, and post-processing histories. This work addresses that bottleneck by developing and validating an end-to-end process chain, from parameter optimization to thermal conversion and matched mechanical testing, with explicit attention to reproducibility, environmental sensitivity, and microscale strengthening.

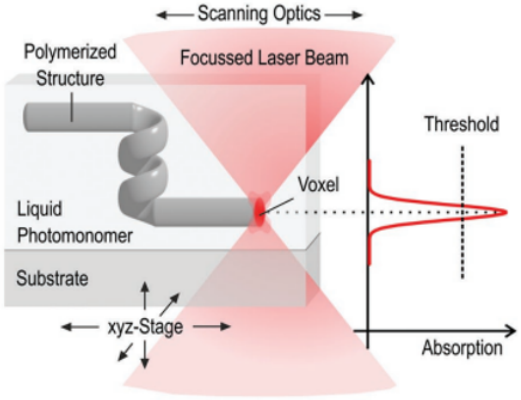

Figure 1: Schematic representation of Two-Photon Polymerization (2PP) and voxel formation, illustrating how nonlinear absorption confines polymerization to a focal voxel and how dose and voxel overlap control feature fidelity. Adapted from [5]

2. Objectives and Scope

Although interest in 2PP-derived silica microstructures is increasing, the literature still provides relatively few mechanically benchmarkable datasets for fused silica obtained from GP-Silica followed by thermal conversion, and comparisons are often difficult because the full process chain (design choices, printing parameters, cleaning/development, environmental conditions, and thermal history) is not reported in a consistent and reproducible way. This gap is critical at the microscale, where small variations in geometry, surface state, and boundary conditions can strongly bias the apparent strength and the observed failure mode.

The motivation of this thesis is therefore twofold: to expand the available experimental evidence by delivering a reference mechanical dataset on fused silica micropillars produced specifically by 2PP and thermal conversion, and to provide an end-to-end process playbook that links upstream fabrication decisions to the final mechanical response. Within this framework, mechanical testing is used as the validation step that justifies the upstream optimization and enables meaningful comparison with fused silica benchmarks.

Accordingly, the work is organized around three pillars: (1) design and 2PP fabrication, including identification of a stable printing window and the definition of practical boundary conditions (time drift and relative humidity) required to achieve reproducible, mechanically testable geometries; (2) post-processing and thermal conversion, optimizing peak temperature and dwell time while tracking shrinkage and morphology evolution to define a reference densified state; and (3) mechanical characterization, combining microcompression and pillar splitting on matched pillar populations to quantify stiffness/strength and an effective fracture toughness, thereby validating the overall process chain and assessing microscale strengthening.

3. Materials and Methods

All experiments were carried out at EMPA – Swiss Federal Laboratories for Materials Science and Technology (Thun, Switzerland). The work followed an end-to-end workflow that connects microfabrication, development, thermal conversion, geometry metrology, and mechanical testing on the same substrate population. Printing was performed in a cleanroom environment to reduce particulate contamination and uncontrolled surface fouling, which are critical at the micrometer scale because they can affect both adhesion during fabrication and defect populations that later dominate strength scatter.

Substrate preparation and 2PP printing. The substrates were silicon chips. Prior to printing, the substrates were cleaned to remove organic and particulate residues (solvent cleaning with isopropanol), then plasma treated to increase surface energy and improve adhesion of the printed structures. Microstructures were fabricated using a Nanoscribe system operated in dip-in configuration (DiLL), i.e., an inverted optical arrangement where the objective is located below the substrate and the polymerization is initiated at the substrate interface to ensure reliable anchoring and stable growth of features. The experimental campaign began with purely polymeric resins (IP-S and IP-Dip) to es-

tablish a consistent "dose logic" and to map the coupled influence of laser power (LP), scan speed (SS), hatching distance (HD), and slicing distance (SD) on print quality and process stability. After this calibration phase, cylindrical micropillar arrays were produced using the silica-loaded GP-Silica resin.

Development and solvent exchange. After printing, samples were developed using methanol as primary developer. To minimize mechanical damage and detachment of fragile pillars, development and rinsing were performed via gentle solvent exchange: the sample was immersed in methanol, then transferred to isopropanol, and finally air-dried without forced flow. This sequence was chosen to limit capillary stresses and handling-induced failure during drying.

Thermal conversion and process screening. Printed GP-Silica structures were converted into fused silica through an integrated debinding+sintering thermal program up to 1300 °C, without an intermediate holding step at 600 °C. The thermal study varied the peak temperature (1100 °C to 1300 °C) and the holding time at 1300 °C (40 min to 215 min) to decouple densification requirements from time-dependent viscous shape relaxation. Based on the combined outcomes in terms of densification and morphology retention, a reference condition of 1300 °C for 4320 s (72 min) was selected as the best compromise between dense-glass formation and geometric fidelity.

Morphological characterization and mechanical testing. Geometry was monitored by SEM at multiple checkpoints: after printing (polymer state), after thermal conversion (glass state), and after mechanical testing to inspect fracture surfaces and identify the dominant failure mode. For each mechanically tested pillar, the post-sintering height h_0 (tilt-corrected when extracted from tilted SEM views), the mean and top diameter D_{top} (used for stress conversion) were measured to contextualize specimen-to-specimen variability and propagate dimensional uncertainty into stress-based metrics. Mechanical characterization consisted of microcompression and pillar-splitting tests on the same pillar populations used for morphological screening, enabling direct links between process conditions, final geometry/defects, and measured mechanical response.

4. Process Window and Environmental Sensitivity

The printing results show a clear transition from "parameter-limited" behavior in polymeric resins to "boundary-condition-limited" behavior in GP-Silica. In IP-S/IP-Dip, LP–SS mapping confirmed a strong coupling between power and writing speed: higher SS requires higher LP to maintain stable polymerization, while low SS narrows the margin to overexposure. Overlap parameters further constrained morphology: increasing HD reduces lateral voxel overlap and can generate scan-line ridges and weak inter-line bonding, whereas excessively small SD can promote cumulative exposure and defects due to repeated passes through the same volume. This polymeric phase provided a transferable interpretation framework: stable printing exists only within finite coupled windows in (LP, SS, HD, SD), and printability is governed by effective dose and voxel overlap rather than by any single parameter.

When moving to GP-Silica, the dominant limitation shifted to a trade-off between adhesion at the substrate interface and a height-amplified axial overgrowth. Tall pillars required high-dose conditions to survive development, but those same conditions activated an instability that produced disproportionate axial growth and tip distortions. Attempts to solve adhesion geometrically (e.g., enlarged bases) improved survival but introduced base overgrowth and filleting that eroded a well-defined cylindrical gauge section, compromising stress conversion and specimen comparability. The strategy therefore converged to a simpler and more interpretable solution: a controlled exposure scheme that strengthens only the first layers at the interface while keeping the pillar core at a moderated dose, combined with progressive downscaling of the target geometry. This downscaling is the key operational lever: reducing height suppresses the height-driven instability and enables printing in a regime where geometry is "reproducibility-limited" rather than "failure-limited".

The final mechanically relevant geometry was a 15×30 µm-class pillar design, where gross failures (missing pillars and extreme overgrowth) were largely suppressed. A representative example of the resulting *as-printed* (post-

development) geometry selected for thermal conversion is shown in Figure 2. For clarity, the main GP-Silica printing parameters used for the final mechanically relevant pillar geometry are summarized in Table 1. However, at this scale, reproducibility becomes sensitive to small perturbations in effective dose, and residual geometric variability manifests primarily as height scatter, taper differences, and dispersion in D_{top} (critical because $\sigma \propto 1/D_{\text{top}}^2$). In this narrow-margin regime, environmental conditions become first-order boundary variables. Two effects were found to be decisive: time drift within a session (progressive loss of cylindricity, rougher top surfaces, and parasitic polymerized artifacts) and relative humidity (RH). Above ∼60% RH, reproducible fabrication became unreliable for the present geometry, whereas 22–55% RH supported stable printing provided that mechanically relevant arrays were prioritized early in the session. These constraints were explicitly adopted as specimen-selection rules for the final mechanical dataset.

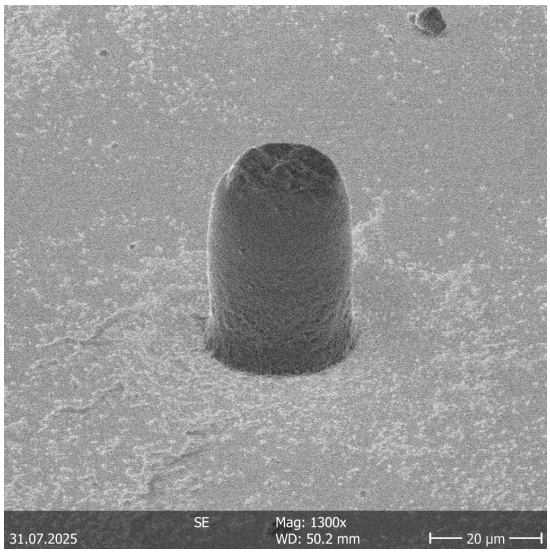

Figure 2: Representative GP-Silica micropillar (15×30 µm) after development, showing the as-printed geometry selected to enter the thermal conversion step.

Parameter	Value
Laser power, LP	≈ 70 mW
Scan speed, SS	≈ 10 mm/s
Hatching distance, HD	≈ 0.2 µm
Slicing distance, SD	≈ 0.6 µm

Table 1: Main GP-Silica printing parameters used for the representative 15×30 µm-class micropillars.

5. Thermal Conversion and Geometric Evolution

Thermal conversion governs both the final material state (density, glass network quality) and the final test geometry (shrinkage and viscous relaxation). Peak-temperature screening showed that temperatures below 1300°C did not reliably yield a dense, smooth fused-silica morphology, while 1300°C produced uniform, fully sintered pillars suitable for quantitative mechanics. The conversion also revealed substrate pinning: the base region remained near its initial footprint while the pillar body contracted, producing a non-self-similar shrinkage field (i.e., not a simple uniform scale-down) that affects stress conversion and fracture boundary conditions.

At fixed peak temperature (1300°C), holding time mainly reshaped the pillar geometry rather than further densifying it. Short dwells (40–72 min) preserved near-cylindrical pillars, while longer dwells (≥120 min) induced rounding, top curvature, and base bulging, consistent with surface-energy-driven viscous flow in fused silica at high temperature under a pinned base. Because these geometric changes influence flat-punch contact, local stress concentrations, and crack initiation, the reference state for mechanical testing was set at 72 min (4320 s) to limit relaxation-driven ambiguity while ensuring a dense-glass benchmark. A representative pillar in this reference state is shown in Figure 3.

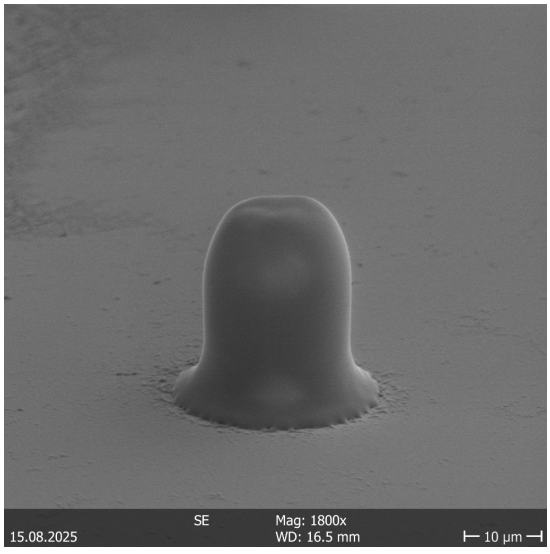

Figure 3: Representative fused silica micropillar after thermal conversion prior to mechanical testing.

6. Mechanical Characterization

Mechanical testing was performed on the reference state (1300°C – 4320 s) using microcompression and pillar splitting on matched pillar populations, enabling a coherent interpretation of stiffness/strength and fracture metrics within the same conversion history.

Microcompression. Load–displacement curves were reduced to engineering stress–strain using the post-sintering top diameter D_{top} and height h_0:

$$\sigma = \frac{F}{A_{\text{top}}}, \qquad A_{\text{top}} = \frac{\pi D_{\text{top}}^2}{4}, \tag{2}$$

$$\varepsilon = \frac{\Delta h}{h_0}. \tag{3}$$

A consistent strain-origin alignment was applied to mitigate toe/compliance artefacts. Stiffness was benchmarked from the most reliable quasi-linear regime (incremental slope plateau), and yield was defined through the 0.2% offset construction to provide an objective criterion for the smooth elastic-to-nonlinear transition typical of amorphous silica micropillars. [6] The population reached multi-GPa peak stresses, substantially exceeding typical macroscopic fused silica strengths; this is consistent with reduced flaw sampling at small scale and with the probabilistic rationale captured by Eq. (1). Importantly, the analysis makes explicit that uncertainty in D_{top} propagates strongly into stress through the $1/D_{\text{top}}^2$ dependence, so geometric variability (taper and top rounding) is a first-order contributor to scatter in σ_y and $\sigma_{\max}$.

Pillar splitting. Pillar splitting was used as a fracture-dominated counterpart, identifying a critical load from the main irreversible load drop and converting it into an effective fracture toughness through a gauge-factor framework:

$$K_c = \gamma \frac{P_c}{R^{3/2}}, \tag{4}$$

where P_c is the critical splitting load, R is the pillar radius (treated carefully for tapered specimens), and γ is a calibration factor. A central methodological feature of this thesis is that γ was determined using stiffness and yield-related inputs extracted from microcompression on the same reference population, so the fracture analysis is internally consistent with the measured mechanical state rather than relying on an unrelated calibration set. The resulting mean effective toughness was

$$K_c \approx 0.65 \text{ MPa}\sqrt{\text{m}},$$

which is consistent with dense fused silica benchmarks and therefore validates both the conversion state and the coupled mechanical methodology.[7]
Importantly, the observed failure morphology systematically deviated from the idealized "three symmetric fragments" splitting pattern often assumed in the theoretical description. In the present pillars, one portion frequently remained attached to the substrate, while one or two fragments detached from the upper region. Post-mortem SEM inspection indicates that the dominant crack did not propagate all the way down to the base; instead, it initiated near the contact region and deviated outward, reaching the free surface at a characteristic height above the substrate (Figure 4). Experimentally, this characteristic height was found to correlate with the force peak: a longer effective crack path (corresponding to a larger detached pillar segment) was associated with a higher maximum load, whereas shorter paths produced lower peaks. The example in Figure 4 shows a typical case where two fragments detach while a bottom segment remains pinned to the substrate.

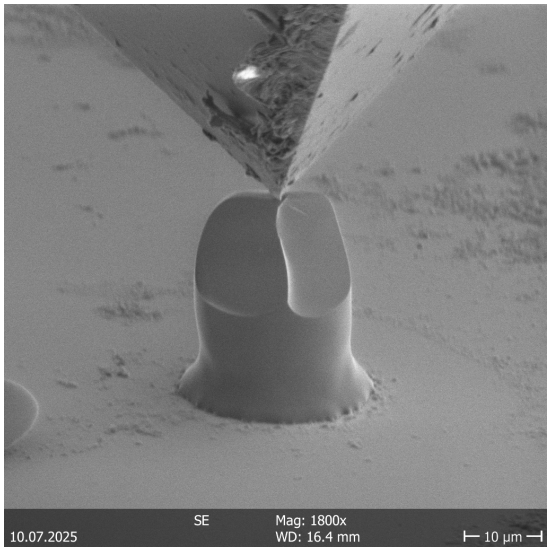

Figure 4: Pillar splitting: two fragments detach while a base segment remains attached.

7. Discussion

The results demonstrate that microscale mechanical performance in 2PP-derived fused silica is strongly process-dependent, not only through nominal print parameters but also through boundary conditions that become decisive near the lower feature-size limit. In GP-Silica, adhesion requirements and a height-dependent axial overgrowth impose a practical geometry downscaling strategy; once pillars reach the 15×30 µm scale, the process becomes reproducibility-limited and environmental sensitivity (time drift and RH) must be treated as a first-order control variable. Thermal conversion further reshapes the test geometry through shrinkage and viscous relaxation, so a reference state must be selected to balance densification with dimensional fidelity. Within that reference state, microcompression delivers a stiffness/strength benchmark approaching dense fused silica expectations, while pillar splitting yields a fracture metric consistent with literature values. The cross-consistency is not incidental: it reflects an intentionally integrated methodology in which microcompression-derived parameters support the fracture calibration, enabling a coherent interpretation of strength and toughness within the same processing state.
Finally, the extracted mechanical properties provide a compact quantitative benchmark for 2PP-derived fused silica micropillars in the selected reference conversion state: the Young's modulus is $E \approx 72$ GPa, the compressive yield stress is $\sigma_y \approx 7.81$ GPa, and the peak compressive strength reaches $\sigma_{\max} \approx 9.63$ GPa. In parallel, pillar splitting yields an effective fracture toughness of $K_c \approx 0.65$ MPa$\sqrt{\text{m}}$, consistent with dense fused silica benchmarks. Together, these values support the "smaller is stronger" strengthening trend in compression while confirming that, once densified, the fracture resistance remains in the expected fused-silica range.

8. Conclusions

This thesis establishes a reproducible end-to-end protocol to fabricate and mechanically test fused silica micropillars produced by 2PP in GP-Silica and subsequent thermal conversion. The main outcomes are: (i) identification of a stable GP-Silica process window through a dose/overlap logic transferred from polymeric mapping and validated via progressive geometry downscaling, (ii) quantification of time drift and relative humidity as first-order boundary conditions near the lower feature-size limit, (iii) definition of a reference thermal conversion state (1300°C – 4320 s) that balances dense-glass formation with geometric fidelity, and (iv) coupled mechanical characterization via microcompression and pillar splitting on matched pillar populations. The obtained effective fracture toughness ($K_c \approx 0.65$ MPa$\sqrt{\text{m}}$) is consistent with dense fused silica benchmarks, supporting the validity of the developed process chain and providing quantitative microscale data for 2PP-derived fused silica structures.

9. Bibliography

References

[1] Felix Kotz, Alexander S. Quick, Patrick Risch, et al. Two-photon polymerization of nanocomposites for the fabrication of transparent fused silica glass microstructures. *Advanced Materials*, 33(9):2006341, 2021.

[2] John B. Wachtman. *Mechanical Properties of Ceramics*. Wiley, 1996.

[3] W. Weibull. A statistical distribution function of wide applicability. *Journal of Applied Mechanics*, 18:293–297, 1951.

[4] Thomas Doualle, Jean-Claude André, and Laurent Gallais. 3d printing of silica glass through a multiphoton polymerization process. *Optics Letters*, 46(2):364–367, 2021.

[5] Jens Bauer, Lucas R. Meza, Tobias A. Schaedler, Ruth Schwaiger, Xiaoyu Zheng, and Lorenzo Valdevit. Nanolattices: An emerging class of mechanical metamaterials. *Advanced Materials*, 29(40):1701850, 2017.

[6] Remo N. Widmer, David Bischof, Jakub Jurczyk, Markus Michler, and Jakob Schwiedrzik. Smooth or not - a guide for accurate measurement of mechanical properties of micropillars. *Materials & Design*, 204:109670, 2021.

[7] Sebastian Bruns, Laszlo Petho, Christian Minnert, Johann Michler, and Karsten Durst. Fracture toughness determination of

fused silica by cube corner indentation cracking and pillar splitting. *Materials & Design*, 186:108311, 2020.